CARRIER POSITION THIRD AND FIFTH ORDER IMDS OF A RADIO-OVER-FIBRE SYSTEM LASER

(Date received: 2.6.2006)

Lisa Yong[1], Mohamad Kadim Suhaidi[2] and Awangku Abdul Rahman Pgn. Hj. Yusof[3]

[1,2,3] School of Engineering, Swinburne University of Technology (Sarawak Campus), Jalan Simpang Tiga, 93576 Kuching, Sarawak

E-mail: lyong@swinburne.edu.my.[1] and kadim@utem.edu.my.[2]

ABSTRACT

The third order intermodulation distortion (IMD_3), instead of the fifth order intermodulation distortion (IMD_5), is often thought to limit the performance of the radio-over-fibre system as it tends to fall in-band. A frequency plan based on the Golomb Ruler is suggested to overcome this IMD_3 problem. However, its effect on the IMD_5 is not known. A laser model is derived based on Volterra Series with electrical parasitics included to simulate the IMD_3 and IMD_5 appearing at carrier position when the channels to be used are in accordance with the Golomb Ruler's marks and compare them with those generated by equally spaced carriers at the maximum RF input level supported by a low and high bias current for the number of channels to be used. The IMD_5 is found to be more dominant than the IMD_3 for the equally spaced frequency plan when the low bias current was employed. The opposite was observed at high bias current. The Golomb Ruler based frequency plan led to no IMD_3s but low levels of IMD_5 were still present at the channels designated for use when both bias currents were employed but they were lower than those due to the equal frequency spaced channels.

Keywords: *Fifth Order Intermodulation Distortions, Golomb Ruler and Third Order Intermodulation Distortions*

1.0 INTRODUCTION

The radio-over-fibre system is an analogue fibre optic system that is used to transport free space radio signals, which can be fixed or mobile wireless. Therefore it is also known as the hybrid radio fibre system [1,2]. The configuration for this system is indicated in Figure 1.

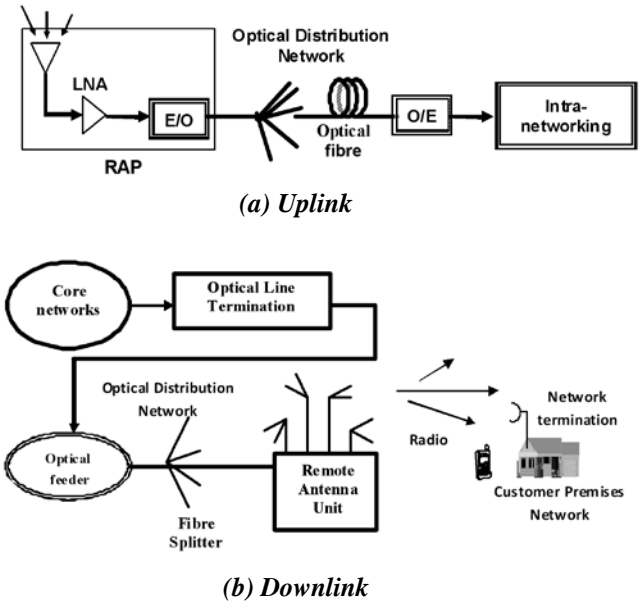

Figure 1 : Basic configurations of the radio-over-fibre system [1]

The free space radio signals from the subscribers, in the uplink, are intercepted by the antenna of the radio access point (RAP) and fed to the low noise amplifier (LNA). The output of the LNA is used to modulate the electric-to-optical converter (E/O). The light output of the E/O is transported using the optical fibre to the central station, where it is detected by the optical-to-electric converter (O/E). The recovered signal goes through further processing in the intra-networking stage [1].

When the signals from the core networks are to be simulcasted or sent to the subscribers, the downlink is referred to. Signals from the core networks can be used to direct modulate the laser if the operation at low frequency is desired. If the transmission is at higher frequencies, the dual frequency optical source must be employed, as indicated in Figure 2.

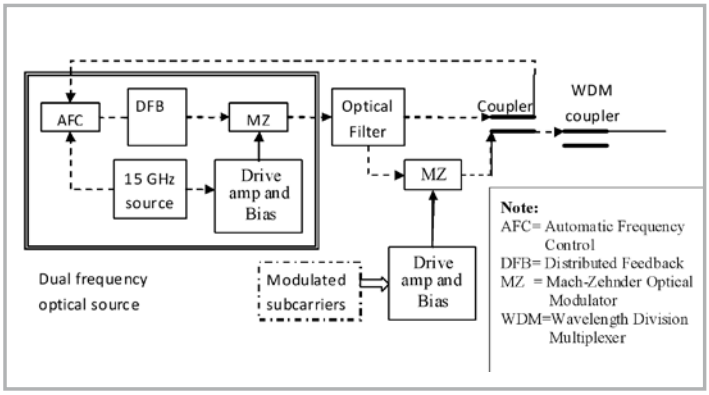

Figure 2 : Dual frequency optical source for 30 to 60GHz transmission [2,3]

The core networks signals must be used to modulate the millimeter wave first. Then the modulated outcome is fed to the optical modulator together with the output of the laser diode or the output of the dual frequency optical source [3]. The light output from the optical modulator is fed to the optical fibre of the optical distribution network through the optical line termination. The other end of the optical fibre is located at the RAP, where the optical signal is converted back to electrical signal and radiated or simulcasts through the remote antenna unit to be intercepted by the antennas of the subscribers' equipment in their premises.

One of the challenges in implementing radio-over-fibre system that serves the mobile communications is to ensure the wide dynamic range of the wireless mobile environment is met by the optical portion of this hybrid fibre radio system. This is essential especially in the uplink of the system as mobile signals intercepted can be very weak when it is at the edge of the cell or very strong when it is close to the base station. The space loss in the micro-cell environment depended on $\frac{1}{\lambda^2}$ and is given by $20\ log\left(\frac{4\pi d}{\lambda}\right)$, where d is the distance from the base station and λ is the wavelength of the mobile station signal [4]. For a 300m radius microcell providing GSM (890 to 915MHz) coverage, the space loss is about 80dB. This means that the dynamic range should be larger than 80dB as the mobile station can be positioned near the base station or at the cell edge [5]. As the input to the base unit of the base station should replicate the weak and strong mobile signals intercepted at the RAP, the optical link of the radio-over-fibre system must not introduce distortions at levels that would cause the mobile signals to be below the detection threshold at the receiver side.

The dynamic range can be limited by the third order intermodulation distortions (IMD_3) of type $2f_1$-f_2 and f_1+f_2-f_3 as they are liable to fall in-band as compared to the second orders distortions for narrowband systems [2]. The E/O conversion stage in the radio-over-fibre system is identified as one of the contributors to this distortion [1]. The IMD_3 can be reduced by rearranging the channels to be used according to the frequency plans in [6] and [7]. As the mobile communication system has to follow certain frequency management or channel assignment scheme and is subjected to interference issues such as co-channel interference [5], the frequency plan being exercised cannot be simply altered to reduce the IMD_3 generated by the E/O conversion.

The signal extraction with frequency arrangement (SEFA) and signal level compression (SLC) had been recommended as means to improve the dynamic range. The SEFA technique, in Figure 3, involves extracting the desired channels from the radio signals with frequencies f_1 to f_4 intercepted by the Main and Sub antenna of the RAP and reassigning them with new frequencies f_1' and f_2' that are no longer adjacent and could reduce the IMD_3 [1], [8] before feeding them to the E/O.

The SLC technique, in Figure 4, is basically used to boost the low-level channels intercepted by the antenna system of the RAP [9] before feeding them to the E/O. The SLC has a compressor that compresses or reduces the dynamic range by elevating the minimum permissible power level to a higher level while maintaining the high-level power channels at their existing levels. Initially, the signal intercepted with the dynamic range Δx or between P_{min} and P_{max} will be fed to the receiver. The receiver, having a dynamic range of Δx_1, will produce an output with power levels between P_{min1} and P_{max1}. Conventionally, Δx is similar to Δx_1 and P_{max} is the same as P_{max1}.

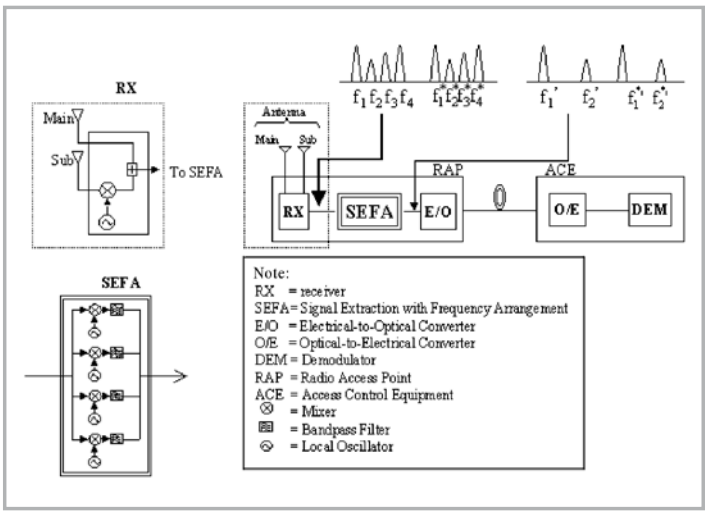

Figure 3 : SEFA technique [8]

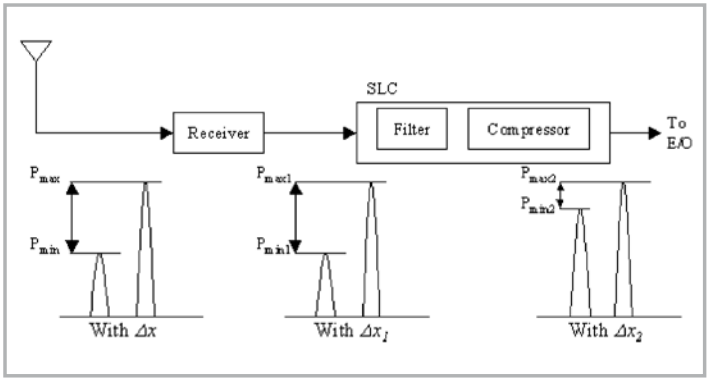

Figure 4 : SLC technique [9]

In a system without the SLC, the output of the receiver or RF amplifier would be used directly to modulate the E/O. This would cause the channel with low power levels to remain weak and be more susceptible to the noise contributed by the optical link than the channel with higher power levels. If the SLC is employed, the channel with P_{min} received by the antenna of the RAP will appear as P_{min2}, which is higher than the P_{min1} input to E/O without the SLC [9]. Thus, elevating the carrier-to-noise ratio for the low-level channel intercepted at the O/E output if the noise or distortion levels did not increase with the raise in channel power level. However, increasing the low-level power channel would elevate the inter-modulation distortion level in other channels. Therefore, the SLC should be deployed together with the SEFA technique.

In order for the SEFA scheme to be implemented, a frequency plan by which the intercepted signals are rearranged should be provided. A frequency plan can be generated through the use of multiple insert delete algorithms where the carriers in the channel with the most number of IMD_3 are deleted and shifted to channels having or leading to best IMD_3 improvement [7] but the IMD_3, though lowered in quantity, might still be considerably high in dBm. Hunziker suggested arranging the channels to be used in an unequal manner by employing the Golomb Ruler in [2] as it avoids IMD_3 from appearing at the

these channels. The Golomb Ruler is a set of non-negative integers or marks such that the distance between any pair of marks are unique and it begins with '0' [10], [11]. The Optimum Golomb Ruler (OGR) is a Golomb Ruler that gives the shortest length for a given number of marks [11]. The OGR for five marks is indicated in Figure 5.

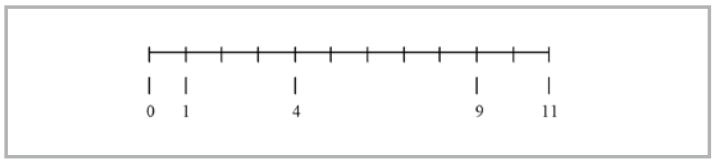

Figure 5 : The Golomb Ruler for five marks

Though arranging the channels to be used according to the Golomb Ruler's marks can lead to zero IMD_3 at carrier position, other intermodulation distortions (IMD) might be present at the carrier positions when the used channels are arranged according to the Golomb Ruler's marks. Therefore the objectives of this paper is to present a radio-over-fibre system laser model derived using Volterra Series and compute the IMD_3 as well as fifth orders intermodulation distortions (IMD_5) appearing at carrier positions when the Golomb Ruler frequency plan (GRFP) and equal frequency spacing (EQSP) are employed for the primary-GSM carriers ranging between 890 and 915MHz with maximum RF input level supported by given bias currents. The IMD_5 is investigated because it is the next odd order distortion after IMD_3. Individual IMD_5s might be insignificant as compared to the IMD_3s but their levels might escalate if their quantities increase and the input magnitude intensifies as the distortions often increase with the input levels. The IMD_5 could rise by the power of five of its input level as compared to the IMD_3 that increases by the power of three. A recent technique used to linearising the IMD_3 is the optoelectronic method [12] and optical injection locking [13]. The optoelectronic method is similar to predistortion method proposed in [14], where the optical signal is converted to electrical signal and uses it to combine with the transmitted RF signal to reduce the IMD_3. The second method involves modulating a master (MLD) and a slave (SLD) laser diodes under injection locking with RF signals. The amplitude and phase of the RF signals are tuned before supplying it to the MLD. The MLD output is fed to the SLD, where residual amplitude modulation suppression takes place. The RF signals from MLD and SLD are added and causes the IMD_3 to reduce [13]. These techniques are still being investigated whereas reducing IMDs using frequency planning in SEFA with SLC permits existing or off the shelves technologies to be deployed.

2.0 VOLTERRA SERIES LASER MODEL

The laser diode's behavior can be described by the single mode laser rate equation pair as given in Equations (1) and (2) [14], [15]. This indicates the laser diode is a dynamic system, which contains energy storing elements. Thus a dynamic system is a system with memory.

$$\frac{dN(t)}{dt} = \frac{I}{qV} - \frac{N(t)}{T_s} - g_0\left(N(t) - N_0\,(1-\varepsilon S(t))\right)S(t) \tag{1}$$

$$\frac{dS(t)}{dt} = \Gamma g_0\left(N(t) - N_0)(1-\varepsilon S(t)\right)S(t) + \Gamma\beta\frac{N(t)}{T_s} - \frac{S(t)}{T_p} \tag{2}$$

where qV is the product of electron charge and active region volume (Am^3s), I is injected current (A), τ_p is the photon lifetime (s), β is the spontaneous coupling coefficient, Γ is the optical confinement factor, ε is power gain compression parameter (m^3), τ_s is the carrier lifetime (s), N_0 is the transparent carrier density (m^{-3}), g_0 is the optical power gain (m^3s^{-1}), N(t) is the carrier density (m^{-3}) and S(t) is the photon density (m^{-3}).

The single mode laser rate Equations can be rearranged and combined to give an output to input relation as given in Equation (3):

$$\frac{I_0 + i_m(t)}{qV} = \frac{N_0}{\tau_s} + \left\{\frac{d\left(S_b + s(t)\right)}{dt} + \frac{\left(S_b + s(t)\right)}{\tau_p} - \Gamma\beta\frac{N_0}{\tau_s}\right\}$$
$$\left(\frac{1}{\Gamma} + \frac{1}{\tau_s}\left(\frac{1-\beta}{\Gamma g_0(1-\varepsilon\left(S_b + s(t)\right)\left(S_b + \Gamma\frac{\beta}{\tau_s}\right)}\right)\right) +$$
$$\frac{d}{dt}\left\{\left(\frac{1}{\Gamma g_0(1-\varepsilon\left(S_b + s(t)\right) + \tau_p\frac{\Gamma\beta}{\tau_s})}\right)\left\{\frac{d\left(S_b + s(t)\right)}{dt} + \frac{\left(S_b + s(t)\right)}{\tau_p} - \Gamma\beta\frac{N_0}{\tau_s}\right\}\right\} \tag{3}$$

where I_0 and $i_m(t)$ are the laser bias and modulating currents. S_b and $s(t)$ are the laser steady-state photon density and photon density due to the modulating current.

The $\frac{1-\beta}{\Gamma g_0(1-\varepsilon\left(S_b + s(t)\right)(S_b + \Gamma\frac{\beta}{\tau_s})}$ and $\frac{1}{\Gamma g_0(1-\varepsilon\left(S_b + s(t)\right) + \tau_p\frac{\Gamma\beta}{\tau_s})}$ terms in Equation (3) can be expanded using Taylor Series. This signifies that the system is weakly nonlinear. Volterra Series is used to model weakly nonlinear systems with memory [16]. When the laser diode is represented by Volterra Series, its output $s(t)$ is expressed as [15]:

$$s(t) = \sum_{n=1}^{\infty}\int_{-\infty}^{\infty}\cdots\int_{-\infty}^{\infty} h_n(u_1\ldots u_n).\prod_{l=1}^{n} i(t-u_l)du_l\ldots du_n \tag{4}$$

where $h_n(u_1, \ldots, u_n)$ is the laser diode's *n-th* order Volterra Series kernel and $i(t)$ is the modulating input signal that represents the intercepted mobile signal in terms of current density.

After performing the mentioned Taylor Series expansion, collecting the terms with $s(t)$ leads to Equation (5) that relates the modulating input with its output [15]:

$$\frac{i_m(t)}{qV} = i(t) = \left[D_1 s(t) + E_1\frac{ds(t)}{dt} + F_1\frac{d^2s(t)}{dt^2}\right] - \left[Ls(t)^2 + Ms(t)\frac{ds(t)}{dt} +\right.$$
$$\left. N_{TF}s(t)\frac{d^2s(t)}{dt^2} + N_{TF}\left(\frac{ds(t)}{dt}\right)^2\right] + \left[Rs(t)^3 + \sigma s(t)^2\frac{ds(t)}{dt} + 2Gs(t)\left(\frac{ds(t)}{dt}\right)^2 +\right.$$
$$\left. Gs(t)^2\frac{d^2s(t)}{dt^2}\right] + \left[Os(t)^4 + Qs(t)^2\left(\frac{ds(t)}{dt}\right)^2 + P_1 s(t)^3\frac{d^2s(t)}{dt^2} + P_2 s(t)^2\frac{ds(t)}{dt}\right]$$
$$+\left[Us(t)^5 + Vs(t)^3\left(\frac{ds(t)}{dt}\right)^2 + Ws(t)^4\frac{ds(t)}{dt} + Xs(t)^2\frac{d^2s(t)}{dt^2}\right] + \ldots \tag{5}$$

In order to solve the above, the exponential growth method or probing method is employed [14, 15, 16] whereby the $i(t)$ in Equations (4) and (5) is substituted with (6):

$$i(t)= \sum_{n=1}^{\infty} e^{j\omega_n t} = e^{j\omega_1 t} + e^{j\omega_2 t} + \ldots + e^{j\omega_n t} \tag{6}$$

Where n is the *n-th* order of the Volterra Series kernel seek and ω_n is the *n-th* angular frequency of the input. This method permits the input to reappear after convolution is performed and the Fourier Transform of the Volterra kernel is also obtained [16], as demonstrated by:

$$\int_{-\infty}^{\infty} h(u)e^{j\omega_1(t-u)}\,du = \int_{-\infty}^{\infty} h(u)e^{j\omega_1 t - j\omega_1 u}\,du = e^{j\omega_1 t}$$

$$\int_{-\infty}^{\infty} h(u)e^{-j\omega_1 u}du = e^{j\omega_1 t}\,H(\omega_1) \tag{7}$$

The Fourier Transform of the first to fifth orders Volterra Series kernels are given by Equations (8) to (12):

$$H_1(\omega_1) = \frac{1}{(D_1 + j\omega_1 E_1 - \omega_1^2 F_1)} = \frac{1}{G_1(\omega_1)} \tag{8}$$

$$H_2(\omega_1, \omega_2) = -\frac{1}{2} = H_1(\omega_1).\, H_1(\omega_2).\, H_2(\omega_1 + \omega_2).\, G_2(\omega_1, \omega_2) \tag{9}$$

$$H_2(\omega_1, \omega_2, \omega_3) =$$

$$-\frac{1}{6G_1\left(\sum_{x=1}^{3}\omega_x\right)}.\left\{\sum_{\substack{k,m,n=1\\ k\neq m\neq n\\ m<n}}^{3} 2H_1(\omega)H_2(\omega_m, \omega_n)G_2(\omega_k, \omega_m + \omega_n) +\right.$$

$$\left. H_1(\omega_1)H_1(\omega_2)H_1(\omega_3)G_3(\omega_1, \omega_2, \omega_3)\right\}. \tag{10}$$

$$H_4(\omega_1, \omega_2, \omega_3, \omega_4) = \frac{1}{24G_1\left(\sum_{x=1}^{4}\omega_n\right)}\left\{\sum_{\substack{k,l,m,n=1\\ k\neq l\neq m\neq n\\ l<m<n}}^{4} 6H_1(\omega_n)H_3(\omega_1, \omega_m, \omega_n)\right.$$

$$G_2(\omega_k, \omega_1 + \omega_m + \omega_n) + \sum_{\substack{k,l,m,n=1\\ k\neq l\neq m\neq n\\ k<l<m<n}}^{4}\left[4H_2(\omega_n, \omega_1)H_2(\omega_m, \omega_n)G_2(\omega_k + \right.$$

$$\left.\omega_1, \omega_m + \omega_n) + 2H_1(\omega_k)H_1(\omega_1)H_2(\omega_m, \omega_n)G_3(\omega_k, \omega_1, \omega_m + \omega_n)\right] +$$

$$\left. H_1(\omega_1)H_1(\omega_2)H_1(\omega_3)H_1(\omega_4)G_4(\omega_1, \omega_2, \omega_3, \omega_4)\right\} \tag{11}$$

$$H_5(\omega_1, \omega_2, \omega_3, \omega_4, \omega_5) = \frac{1}{120G_1\left(\sum_{x=1}^{5}\omega_n\right)}\left[\sum_{\substack{k,l,m,n,p=1\\ k\neq l\neq m\neq n\neq p\\ l<m<n<p}}^{5} 24H_1(\omega_k)\right.$$

$$H_4(\omega_1, \omega_m, \omega_n, \omega_p)\, G_2(\omega_k, \omega_1 + \omega_m + \omega_n + \omega_p) + \sum_{\substack{k,l,m,n,p=1\\ k\neq l\neq m\neq n\neq p\\ k<l,m<n<p}}^{5}$$

$$\left[12H_2(\omega_k, \omega_l)\, H_3(\omega_m, \omega_n, \omega_p)\, G_2(\omega_k + \omega_1, \omega_m + \omega_n + \omega_p) + 6H_1(\omega_k)\right.$$

$$H_1(\omega_1)\, H_3(\omega_m, \omega_n, \omega_p)\, G_3(\omega_k, \omega_1, \omega_m + \omega_n + \omega_p)\Big] + \sum_{\substack{k,l,m,n,p=1\\ k\neq l\neq m\neq n\neq p\\ k<l,m<n<p}}^{5}$$

$$4H_1(\omega_k)\, H_2(\omega_l, \omega_m)\, H_2(\omega_n, \omega_p)\, G_3(\omega_k, \omega_l + \omega_m, \omega_n + \omega_p) + \sum_{\substack{k,l,m,n,p=1\\ k\neq l\neq m\neq n\neq p\\ k<l,m<n<p}}^{5}$$

$$\left[2H_1(\omega_k)\, H_1(\omega_l)\, H_1(\omega_m)\, H_2(\omega_n, \omega_p)\, G_4(\omega_k, \omega_l, \omega_m, \omega_n + \omega_p) + H_1(\omega_1)\right.$$

$$\left. H_1(\omega_2)\, H_1(\omega_3).\, H_1(\omega_4)\, H_1(\omega_5)\, G_5(\omega_1, \omega_2, \omega_3, \omega_4, \omega_5)\right] \tag{12}$$

Where

$$G_2(\omega_1, \omega_2) = -2K - jM.\,(\omega_1 + \omega_2) + N_{TF}.\,(\omega_1 + \omega_2)^2 \tag{13}$$

$$G_3(\omega_1, \omega_2, \omega_3) = 6R - 2j\sigma.\left[\sum_{x=1}^{3}\omega_x\right] - 2G.\left[\sum_{x=1}^{3}\omega_x\right]^2 \tag{14}$$

$$G_4(\omega_1, \omega_2, \omega_3, \omega_4) = 24O + j6P_2.\left[\sum_{x=1}^{4}\omega_x\right] - 6P_1.\left[\sum_{x=1}^{4}\omega_x\right]^2 \tag{15}$$

$$G_5(\omega_1, \omega_2, \omega_3, \omega_4) = 120U + j24W_2.\left[\sum_{x=1}^{5}\omega_x\right] - 24X.\left[\sum_{x=1}^{5}\omega_x\right]^2 \tag{16}$$

2.1 OPTICAL MODULATION INDEX AND ELECTRICAL PARASITICS

Besides the Fourier Transform of the Volterra Series kernels, the current fed to the laser diode has to be specified to determine the IMDs. The input signal that is fed to the laser diode is affected by its source location. When the signal is originating from the edge of the cell, it can be as low as -120dBm for a cell with 300m radius. If it is around the radio access point, it can be as high as 0 to 39 dBm [5]. The *RF* input power between -120 to 40dBm can translate to between 6.32456×10^{-6} and 632 *mA* of modulating input current (ΔI) according to Equations (17) [17]:

$$\Delta I = \sqrt{\frac{2P_i}{R_i}}. \tag{17}$$

Where *Pi* is the input power and *Ri* is the input resistance of 50Ω. The magnitude of the input current (ΔI) can be expressed as the optical modulation for a carrier mopt by [14]:

$$m_{opt} = \frac{\Delta I}{I_0 - \dot{I}_{th}} \tag{18}$$

Where I_0 and I_{th} are the bias and threshold currents. The range of bias current that can be employed can be determined by solving equation (19), obtained by collecting the steady-state photon density and bias current terms in Equation (3).

$$I_0 = qV\left[\frac{N_0}{\tau_s} + \left(\frac{S_b}{\tau_p} - \Gamma\beta\frac{N_0}{\tau_s}\right)\left(\frac{1}{\Gamma} + \frac{1}{\tau_s}\left(\frac{1-\beta}{\Gamma G_0(1-\varepsilon S_b)S_b + \Gamma\frac{\beta}{\tau_s}}\right)\right)\right] \tag{19}$$

When the input to the laser diode is made up of several carriers, the total modulation index (m_{tot}) needs to be considered. The m_{opt} is related to m_{tot} by [14]:

$$m_{tot} = \sqrt{\sum_{n=1}^{N} m_{opt_n}^{\ 2}} \tag{20}$$

The m_{tot} should be maintained at approximately 1 to avoid overmodulation, which can lead to higher levels of distortions [18]. As the m_{tot} total modulation index is limited to a maximum of 1, the m_{opt} might depend on the number of carriers to be used, which in turn is related to the frequency reuse factor implemented.

The actual current at the active region can be different from anticipated as the current has to pass through the electrical parasitics of the laser diode [19]. Therefore the electrical parasitics should be accounted for in the computation of the intermodulation distortions. The IMD are related to the Fourier Transform of the Volterra Series kernels, the electrical parasitics $P_{elec}(\omega)$ and the modulating signal magnitude using Equation (21) assuming the carriers possess the same magnitude or optical modulation index:

$$IMD\left(\sum a_x \omega_x\right) = \frac{\sum_{x=1}^{N}|a_x|!}{\prod_{x=1}^{N}|a_x|!} \cdot \frac{\Delta I}{2}^{\sum_{x=1}^{N}|a_x|} \cdot \left| H_{\sum_{x=1}^{N}|a_x|}(\pm\omega_1,\ldots \pm\omega_N) \cdot \prod_{x=1}^{N} P_{ara}(\omega_x)^{|ax|} \right| \tag{21}$$

where a_x is the coefficient of the *x-th* tone that generates the required interdmodulation distortion (IMD), $\prod_{x=1}^{N}|a_x|$ represents the order of the IMD and N is the number of tones that make up the IMD.

3.0 FREQUENCY PLANS, SIMULATION ASSUMPTIONS AND PARAMETERS

For this paper, the modulating signal is assumed to be made up of carriers with the same magnitude in the primary-GSM frequencies, which is from 890 to 915*MHz* with a 200*kHz* spacing. This means that 125 carriers can be supported. The channel numbering begins from 1 to 125. According to Wake in [2], the frequency reuse factor greater than 15 or a cluster of more than 15 cells are needed to meet the interference requirement. This means that the 125 carriers will be divided among the cells. For the frequency reuse factor of 20, each cell might be assigned six or seven carriers. Six carriers were employed in the IMD_3 and IMD_5 appearing at carrier positions simulation in this paper. The channel number (*ch_no*) and carrier frequency (f_c) are related using Equation (21).

$$f_{c_n} = 890MHz + ch\_no \times 200kHz \qquad ch\_no_n \tag{22}$$

The Golomb Ruler for six marks in [11] is used to determine the channel used for the GRFP. Table 1 indicates the channel number (*ch_no*) and the carrier frequencies for both the GRFP and EQSP. The Golomb Ruler frequency plan took up about a fifth of the bandwidth occupied by the equally spaced carriers.

Table 1 : Carrier numbers, channel numbers and carrier frequencies for GRFP and EQSP

Carrier Number	EQSP		GRFP	
	Channel Number	Carrier frequency	Channel Number	Carrier frequency
1	1	890.2MHz	1	890.2MHz
2	21	894.2MHz	2	890.4MHz
3	41	898.2MHz	5	891.0MHz
4	61	902.2MHz	11	892.2MHz
5	81	906.2MHz	13	892.6MHz
6	101	910.2MHz	18	893.6MHz

The parameters of the Ortel-1510B and its electrical parasitics in [19] were referred to for the simulation. A summary of the laser diode parameters is given in Table 2. The equivalent circuit and parameters for the electrical parasitics are indicated in Figure 6 and Table 3.

Table 2 : Laser parameters employed in simulation [19]

Parameter	Value
product of electron charge and active region volume, *qV*	1.28 x 10^{-35} (Am^3s)
Laser threshold current, *Ith*	15.1 x 10^{-3} (A)
photon lifetime, τp	1 x 10^{-12} (s)
carrier lifetime, τs	1.6 x 10^{-9} (s)
transparent carrier density, N_0	1 x 10^{-24} m^{-3}
optical power gain, g_0	3.3 x 10^{-12} (m^3s^{-1})
spontaneous coupling coefficient, β	2 x 10^{-3}
optical confinement factor, Γ	0.35
power gain compression parameter, ε	3.2 x 10^{-23} (m^3)

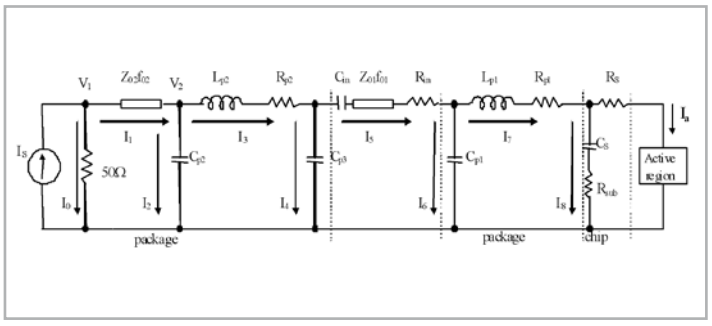

Figure 6 : The equivalent circuit model of Ortel-1510B's electrical parasitics [19]

Table 3 : Parasitics elements employed in simulation [19]

Elements	Value	Elements	Value
C_{p1}	3.0pF	R_{p2}	0.5Ω
L_{p1}	0.14nH	C_{p3}	0.46pF
R_{p1}	1.5Ω	Z_{01}	48.4Ω
R_{sub}	1.5Ω	f_{01}	3.8GHz
C_s	5.6pF	Z_{02}	50.5Ω
R_s	6Ω	f_{02}	5.13GHz
C_{p2}	0.2pF	R_{in}	58.5Ω
L_{p2}	1.3nH	C_{in}	1800pF

Two different simulations were performed. The first assumed a low I_0 of 25*mA* with m_{tot} of 1, which translated to -3.889 dBm per carrier. The second simulation was based on the maximum permissible I_0 of 0.44*A* with m_{tot} of 1, which translated to 28.786dBm per carrier. The mtot of 1 is used to represent maximum dynamic compression in the SLC. In both cases, the m_{opt} is 0.408. The maximum I_0 that can be used with the Ortel-1510B is determined by solving Equation (19) and indicated in Figure 7.

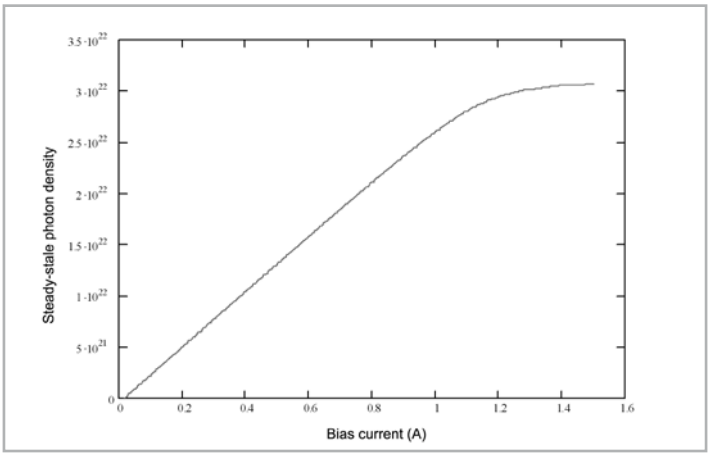

Figure 7 : Steady-state photon density (1/m³) versus bias current

The steady-state photon density is linear for the bias current from approximately 15*mA* until 0.88*A*. Therefore, I_0 ranges between 15 to 0.44*A* (based on mid-point biasing). ΔI must not exceed $I_0 - I_{th}$ to avoid static non-linear distortion, due to clipping at threshold and limiting at saturation [20]. From Equations (18) and (20), I_0 has to be 1.564*A* to support six carriers of 40dBm. As such, the Ortel-1510B cannot support modulating input with RF level of 40dBm with I_0 of 0.44*A*. The maximum RF level that can be supported by this device is 28.786dBm.

4.0 RESULTS AND DISCUSSIONS

4.1 IMD_3 AND IMD_5 QUANTITIES

The IMD_3 and IMD_5 that appeared at carrier position based on simulation are listed in Table 4. Therefore, they were employed in determining the composite IMD_3 and IMD_5 quantity and levels appearing at each channel or carrier used.

Table 4 : Types of IMD_3 and IMD_5 appearing at carrier position

Number of tones	IMD_3 Type	IMD_5 Type
2 (f_1, f_2)	$2f_1 - f_2$	$3f_1 - 2f_2$
3 (f_1, f_2, f_3)	$f_1 + f_2 - f_3$	$3f_1 - f_2 - f_3$ $2f_1 + f_2 - 2f_3$
4 (f_1, f_2, f_3, f_4)		$f_1 + f_2 + f_3 - 2f_1$ $2f_1 + f_2 - f_3 - f_4$
5 (f_1, f_2, f_3, f_4, f_5)		$f_1 + f_2 + f_3 - f_4 - f_5$

The total number of IMD_3s and IMD_5s at carrier positions are indicated in Figure 8. Table 5 indicates the types of IMD_3 and IMD_5 that appeared at carrier position for both frequency plans.

Both the IMD_3 and IMD_5 appeared at the EQSP's used channels. The total number of IMD_3s maximises at the middle used channels following the total number to IMD_3 of type $f_1 + f_2 - f_3$. This type of IMD_3 contributes 66.7 to 77.8% of the total number of IMD_3 for the EQSP. Only two $2f_1 - f_2$ type IMD_3 appeared at all EQSP used channels.

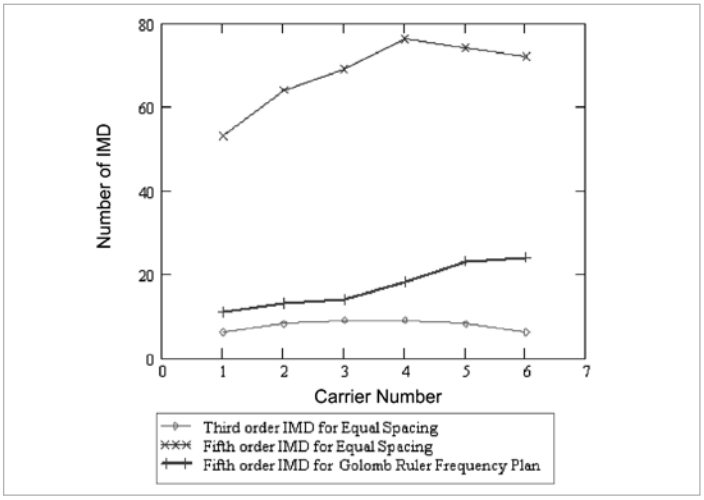

Figure 8 : Total number of IMD_3 and IMD_5 at carrier positions

Table 5 : The types of IMD_3 and IMD_5 at carrier position and their quantities

Type	EQSP						GRFP					
	Carrier Number						Carrier Number					
	1	2	3	4	5	6	1	2	3	4	5	6
$2f_1-f_2$	2	2	2	2	2	2	0	0	0	0	0	0
$f_1+f_2-f_3$	4	6	7	7	6	4	0	0	0	0	0	0
Total IMD_3	**6**	**8**	**9**	**9**	**8**	**6**	**0**	**0**	**0**	**0**	**0**	**0**
$3f_1-2f_2$	1	1	1	1	1	1	0	0	0	1	1	0
$3f_1-f_2-f_3$	5	5	4	4	3	3	1	2	0	0	1	1
$2f_1+f_2-2f_3$	7	7	8	8	7	7	3	1	3	3	3	1
$f_1+f_2+f_3-2f_4$	5	8	9	9	8	5	0	1	1	2	1	1
$2f_1+f_2-f_3-f_4$	21	27	26	31	30	34	5	7	7	7	9	10
$f_1+f_2+f_3-f_4-f_5$	15	16	21	23	25	22	2	2	3	5	8	11
Total IMD_5	**53**	**64**	**69**	**76**	**74**	**72**	**11**	**13**	**14**	**18**	**23**	**24**

The total number of IMD_5s at EQSP used channels is 7 to 12 times higher than that of the IMD_3s. The total number of IMD_5 maximised at the fourth channel used in the EQSP because the number of $2f_1 + f_2 - 2f_3$, $2f_1 + f_2 - f_3 - f_4$ and $f_1 + f_2 + f_3 - 2f_4$ types IMD_5 maximised at this channel. The total number of IMD_5 decreases slightly at the last two channels used as the number of $2f_1 + f_2 - f_3 - f_4$ and $f_1 + f_2 + f_3 - f_4 - f_5$ types IMD_5 are at or near maximum. These types of IMD_5 made up 66 to 78% of total number of IMD_5s in the EQSP.

The GRFP led to zero IMD_3 from falling onto the channel used but some IMD_5s were still present. The $2f_1 + f_2 - f_3 - f_4$ type IMD_5 made up 38 to 54% of the total IMD_5 appearing at the GRFP used channels. This is followed by IMD_5 of type $2f_1 + f_2 - 2f_3$, and $f_1 + f_2 + f_3 - f_4 - f_5$, which contributed 4 to 27.3% and 15 to 46%. The total number of IMD_5s for the EQSP are three to five times higher than the GRFP at all carrier positions. This implies that lower IMD_5 levels might be generated by the GRFP carriers than the EQSP carriers.

4.2 COMPOSITE IMD_3 AND IMD_5 LEVELS

4.2.1 LOW BIAS CURRENT

The composite IMD_3 and IMD_5 levels at carrier positions for both frequency plans at I_0 of 25*mA* are given in Figure 9 and, Tables 6 and 7. The GRFP's composite IMD_3 is not indicated as zero IMD_3 appears at carrier position. EQSP's composite IMD_3 levels maximise at the middle channels. This is contributed mainly by the IMD_3 of type $f_1 + f_2 - f_3$, which makes up 79 to 87.5% of the composite IMD_3 observed. Though there are similar total numbers of IMD_3 at end used channels, the composite IMD_3 levels are higher at higher frequencies channels. The individual IMD_3 level is a function of the resultant frequency by which it appears. Therefore, individual IMD_3 levels are greater at higher frequencies.

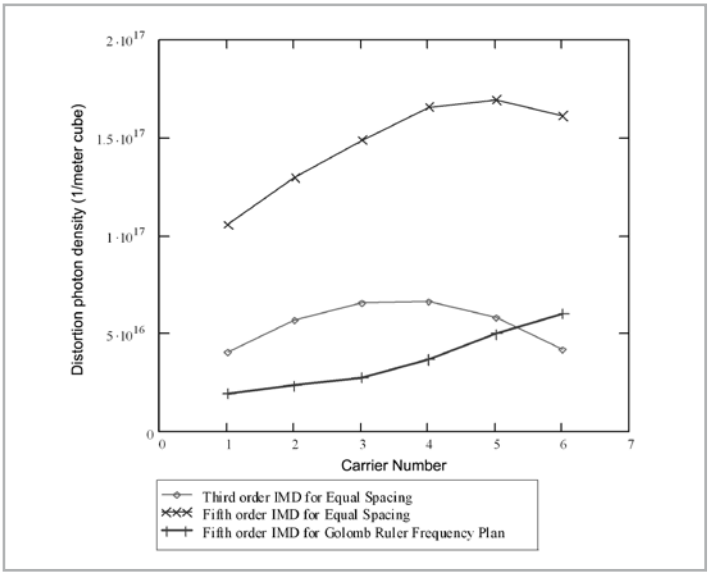

Figure 9 : The carrier positions third and fifth orders IMDs levels at 25mA bias current

The $f_1+f_2+f_3-2f_4$, $2f_1+f_2-f_3-f_4$ and $f_1+f_2+f_3-f_4-f_5$ types IMD_5 contribute 5.7 to 11%, 31.5 to 38% and 44.2 to 54% to the composite IMD_5 levels in EQSP. Though the total number of $f_1+f_2+f_3-f_4-f_5$ type IMD_5 is lower than $2f_1+f_2-f_3-f_4$ type IMD_5, their individual levels are higher. This $f_1+f_2+f_3-f_4-f_5$ type IMD_5 results from carriers with higher frequencies and leads to high individual IMD_5 levels. Though the individual IMD_5 levels are lower than those of IMD_3, its quantity is 7.6 to 12 times larger than the IMD_3 in the EQSP. The EQSP's composite IMD_5 levels are higher than its composite IMD_3 levels. They are 3.27 to 4.8 times higher than the composite IMD_3 levels. This signifies that the IMD_5 is more dominant than the IMD_3 for EQSP at the maximum mtot with low I_0. Therefore, it should not be neglected.

Table 6 : Distortion levels ($10^{14}/m^3$) at EQSP carriers at 25mA

Distortion Type	Carrier Number					
	1	**2**	**3**	**4**	**5**	**6**
$2f_1-f_2$	80.7346	91.268	81.742	82.280	82.570	83.300
$f_1 + f_2 - f_3$	323.04	487.506	572.318	575.833	496.647	333.091
Total IMD_3	**403.775**	**568.774**	**654.060**	**658.113**	**579.403**	**416.389**
$3f_1-2f_2$	2.962	2.981	3.00	3.01	3.03	3.05
$3f_1-f_2-f_3$	29.616	29.7918	23.979	24.1253	18.202	18.302
$2f_1+f_2-2f_3$	62.210	62.577	71.933	72.356	63.679	64.051
$f_1+f_2+f_3-2f_4$	88.869	143.017	161.853	162.798	145.568	91.504
$2f_1+f_2-f_3-f_4$	373.165	482.636	467.58	560.781	545.942	622.350
$f_1+f_2+f_3-f_4-f_5$	497.589	572.066	755.195	832.003	909.661	805.235
Total IMD_5	**1054.41**	**1293.07**	**1483.54**	**1655.08**	**1686.08**	**1604.49**
Total IMDs	1458.185	1861.844	2137.6	2313.193	2265.483	2020.879

Table 7 : Distortion levels ($10^{14}/m^3$) at GRFP carriers at 25mA

Distortion Type	GRFP Distortion Level ($10^{14}/m^3$)					
	Carrier Number					
	1	**2**	**3**	**4**	**5**	**6**
$2f_1-f_2$	0	0	0	0	0	0
$f_1 + f_2 - f_3$	0	0	0	0	0	0
Total IMD_3	**0**	**0**	**0**	**0**	**0**	**0**
$3f_1-2f_2$	0	0	0	2.967	2.969	0
$3f_1-f_2-f_3$	5.917	11.84	0	0	5.939	5.947
$2f_1+f_2-2f_3$	26.63	8.880	26.66	26.71	26.72	8.921
$f_1+f_2+f_3-2f_4$	0	17.76	17.78	35.61	17.81	17.84
$2f_1+f_2-f_3-f_4$	88.76	124.3	123.4	124.6	160.3	178.4
$f_1+f_2+f_3-f_4-f_5$	71.01	71.03	106.6	178.0	285.0	392.5
Total IMD_5	**192.3**	**233.8**	**275.5**	**368.0**	**498.8**	**603.7**
Total IMDs	192.3	233.8	275.5	368	498.8	603.7

For the first three used channels, the $2f_1+f_2-f_3-f_4$ type IMD_5 contributed 46.2 to 53.2% of the composite IMD_5 levels for the GRFP. This is because the total number of $2f_1+f_2-f_3-f_4$ type IMD_5 is twice that of the $f_1+f_2+f_3-f_4-f_5$ type IMD_5. The $f_1+f_2+f_3-f_4-f_5$ type IMD_5 contributed 48.3 to 65% of the composite IMD_5 levels in the last three used channels of the GRFP. These individual IMD_5 levels are higher than that of the $2f_1+f_2-f_3-f_4$ type as they result from carriers of higher frequencies.

The composite IMD_5 levels for the GRFP are between 1.16 to 2.24 times lower than those of the EQSP IMD_3 for the first five used channels. However, the opposite is observed in the last channel. This is because there are four times more IMD_5 appearing at that channels as compared to IMD_3. Thus, signifying though the GRFP led to zero IMD_3, the IMD_5 at carrier positions can still be comparable to the IMD_3 of EQSP at high mtot and low bias current. The composite IMD_5 levels due to the EQSP are 2.66 to 5.53 times higher than those of the GRFP. This indicates that the GRFP is a better frequency plan than EQSP to be implemented with SEFA and SLC with maximum dynamic compression at high mtot and low bias current.

4.2.2 HIGH BIAS CURRENT

The composite IMD_3 and IMD_5 levels in Figure 10 and Table 8 had increased more than 200 times and 77 to 118 time as compared to when I_0 was 0.44A. The Fourier Transform of the third and fifth order Volterra kernels generally decreased by 200 and 5600000 times at 0.44A as compared to 25*mA*. However, the 28.786dBm RF level supported by 0.44A translated to ΔI of 0.1735A, which is 43 times greater than the ΔI supported by 25mA. As such, ΔI^3 at 0.44A is 6.6×10^{40} times greater than that at 25mA. ΔI^5 at 0.44A is 1.46×10^8 times greater than that at 25*mA*. This causes the individual IMD levels to increase, which in turn increases the composite IMD levels.

The composite IMD_3 levels of the EQSP are higher than its composite IMD_5 levels when I0 is 0.44A. This is contributed by the greater decrease the Fourier Transform of the fifth order Volterra kernels encountered and smaller increase in ΔI^5 than that of the third order. As a result, each individual IMD_5 level becomes minute as compared to the IMD_3. Though the total number of IMD_5 is seven to 12 times that of IMD_3, the composite IMD_5 levels are less than half the composite IMD_3 levels.

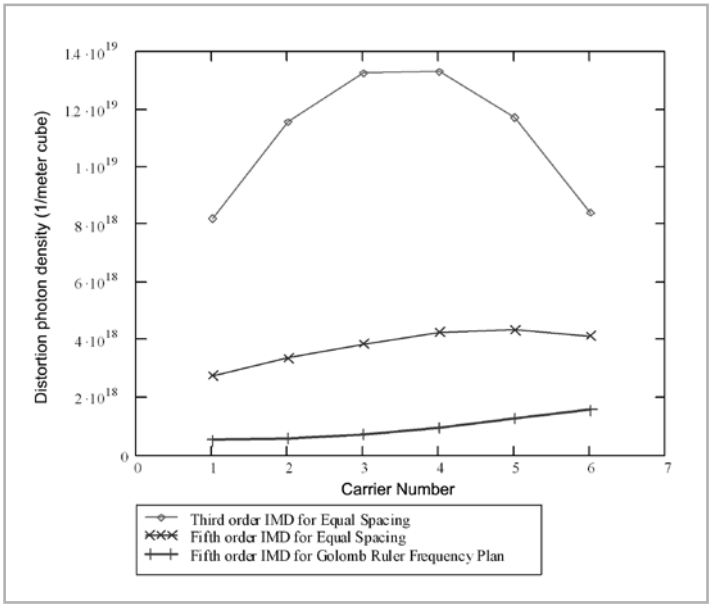

Figure 10 : The carrier positions third and fifth orders IMDs levels at 0.44A bias current

The $f_1+f_2-f_3$ type IMD_3 still contributed highly to the EQSP composite IMD_3 levels, between 80 to 91%. The $f_1+f_2+f_3-2f_4$, $2f_1+f_2-f_3-f_4$ and $f_1+f_2+f_3-f_4-f_5$ types IMD_5 still contributed 91 to 95% of the EQSP composite IMD_5 levels.

Table 8 : Distortion levels ($10^{15}/m^3$) at EQSP carriers at 0.44A

Distortion Type	Carrier Number					
	1	2	3	4	5	6
$2f_1-f_2$	1642.644	1647.446	1657.034	1661.814	1671.425	1676.182
$f_1+f_2-f_3$	6562.613	9892.617	11589.59	16423.3	10020.42	6712.829
Total IMD_3	**8205.26**	**11540.1**	**13246.6**	**18085.1**	**11691.8**	**8389.01**
$3f_1-2f_2$	7.578033	7.7004	7.7226	7.8033	7.8257	7.8479
$3f_1-f_2-f_3$	76.809	77.1487	61.9561	62.1926	46.8383	47.0871
$2f_1+f_2-2f_3$	161.1795	161.91	185.896	186.7232	164.1323	164.864
$f_1+f_2+f_3-2f_4$	230.2804	370.196	418.245	420.15	375.0421	235.4937
$2f_1+f_2-f_3-f_4$	967.795	1249.744	1208.223	1446.936	1405.966	1600.483
$f_1+f_2+f_3-f_4-f_5$	1290.122	1480.78	1952.675	2147.97	2345.036	2072.354
Total IMD_5	**2733.76**	**3347.48**	**3834.72**	**4271.78**	**4344.84**	**4128.13**
Total IMDs	10939.02	14887.54	17081.34	22356.89	16036.69	12517.14

The composite IMD_5 levels for the GRFP at 0.44A in Figure 10 and Table 9 increased 20 times as compared to those at 25*mA*. This increase is mainly due to the increase in ΔI^5 term. The $2f_1+f_2-f_3-f_4$ and $f_1+f_2+f_3-f_4-f_5$ types of IMD_5 still contributed 82.2 to 94.6% of the GRFP composite IMD_5 levels. The composite IMD_5 levels for this frequency plan are 2.63 to 5.49 times lower than those of the EQSP. This indicates that the GRFP is more suitable to be implemented with the SEFA and SLC when high mtot and high bias current are employed.

Table 9 : Distortion levels ($10^{15}/m^3$) at GRFP carriers at 0.44A

Distortion Type	Carrier Number					
	1	2	3	4	5	6
$2f^1-f^2$	0	0	0	0	0	0
$f^1+f^2-f^3$	0	0	0	0	0	0
Total IMD_3	**0**	**0**	**0**	**0**	**0**	**0**
$3f^1-2f^2$	0	0	0	7.7223	7.7260	0
$3f^1-f^2-f^3$	15.4077	30.8142	0	0	15.4434	15.4619
$2f^1+f^2-2f^3$	69.3046	23.1078	69.3924	69.4852	69.5284	23.1964
$f^1+f^2+f^3-2f^4$	0	46.2213	46.2445	92.6335	46.3532	46.4044
$2f^1+f^2-f^3-f^4$	231.09	324.589	323.829	324.241	417.015	463.818
$f^1+f^2+f^3-f^4-f^5$	184.849	184.902	277.578	463.273	741.495	1020.57
Total IMD_5	**500.651**	**609.634**	**717.044**	**957.355**	**1297.56**	**1569.45**

4.3 EFFECTS OF IMD_3 AND IMD_5 ON CARRIERS

The undistorted carriers' magnitudes for both frequency plans are indicated in Figures 11 and 12.

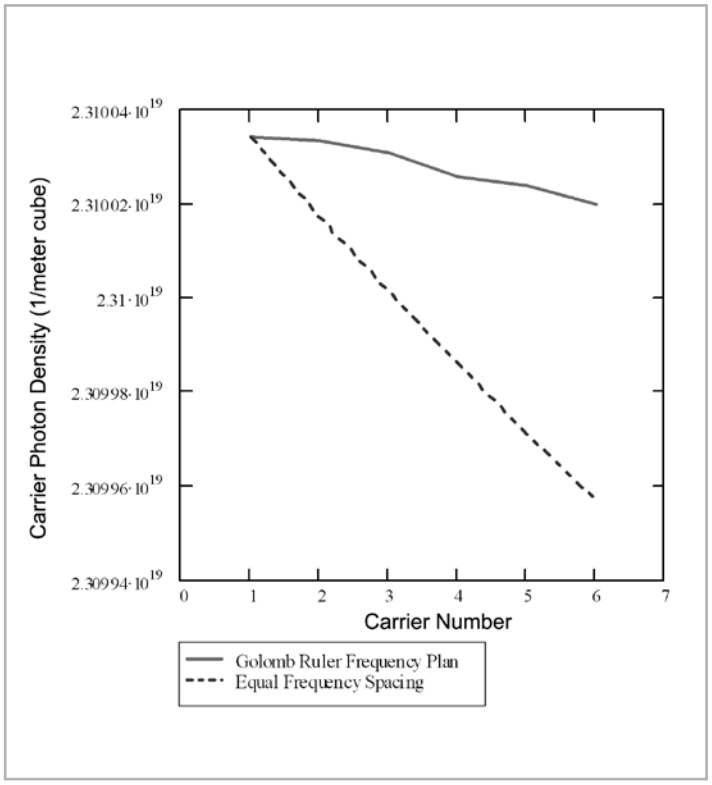

Figure 11 : The undistorted carriers at the bias current of 25mA

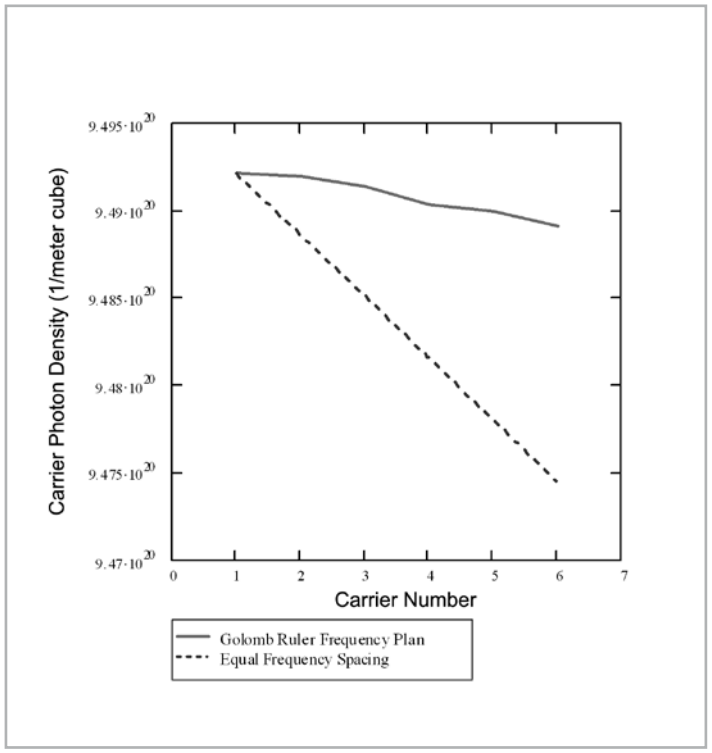

Figure 12 : The undistorted carriers at the bias current of 0.44A

These undistorted carriers decrease with increasing carrier number at both I_0 though their magnitudes were the same at the E/O input. The decrease is because the Fourier Transform of the first order Volterra series kernel decreases for frequencies between 890 to 915*MHz*. As the EQSP used channels are at higher frequencies than those of the GRFP, its undistorted carriers decrease more drastically than those of GRFP. The EQSP carriers' decreases are 5.33 and 5.92 times greater than the GRFP for I_0 of 25*mA* 0.44A.

The distorted carriers for both I_0 are indicated in Figures 13 and 14. The distorted carriers are generally lower than those undistorted.

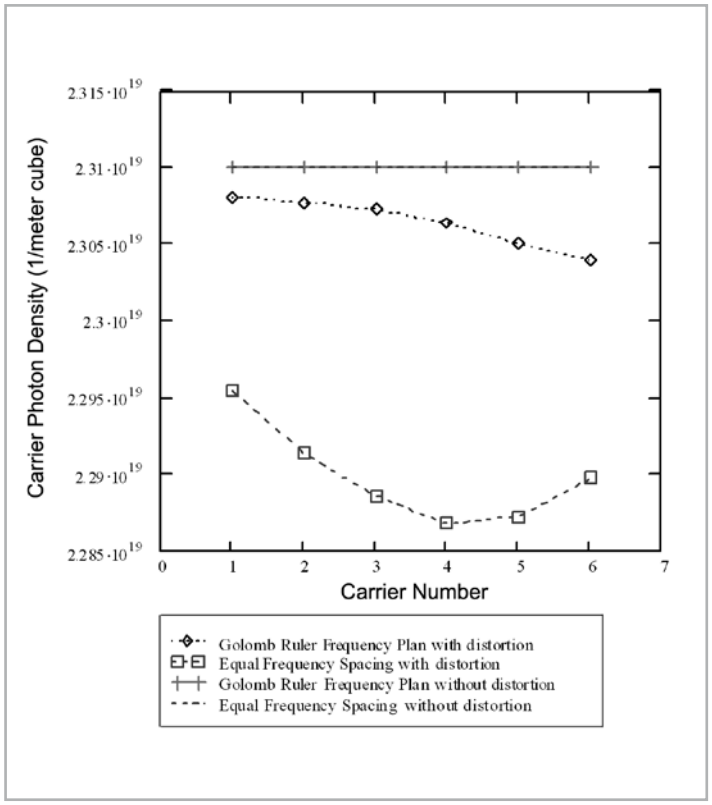

Figure 13 : The distorted and undistorted carriers at the bias current of 25mA

The composite IMD_3 and IMD_5 levels at carrier position lowered the undistorted EQSP carriers by 38 to 61.6% and 1.15 to 2.36% at 25*mA* and at 0.44A. The carriers are less distorted at 0.44A as the increase in the carrier is 30 times greater than the increase of composite IMD_3 and IMD_5 levels. This signifies higher bias current is preferred to low bias current when implementing SLC with maximum dynamic range compression. The composite IMD_5 levels contributed 76.6 to 82.9% of the carrier position IMD levels in the EQSP at 25*mA*. On the other hand, the composite IMD_3 levels contributed 67 to 81% of the carrier position IMD levels in EQSP at 0.44A. The middle used channels are the most distorted channels in the EQSP at 25*mA*. The fourth used channel is most distorted in the EQSP at 0.44A. This is because the composite IMD_3 and IMD_5 levels maximise in these channels.

The GRFP distorted carriers are merely 0.083 to 0.26% and 0.053 to 0.165% lower than its undistorted carriers at 25*mA* and 0.44A. The sixth used channel in the GRFP is the most distorted channel for both bias current cases. The GRFP carriers are generally less distorted as compared to the EQSP mainly because it led to zero IMD_3 and less IMD_5 at carrier positions.

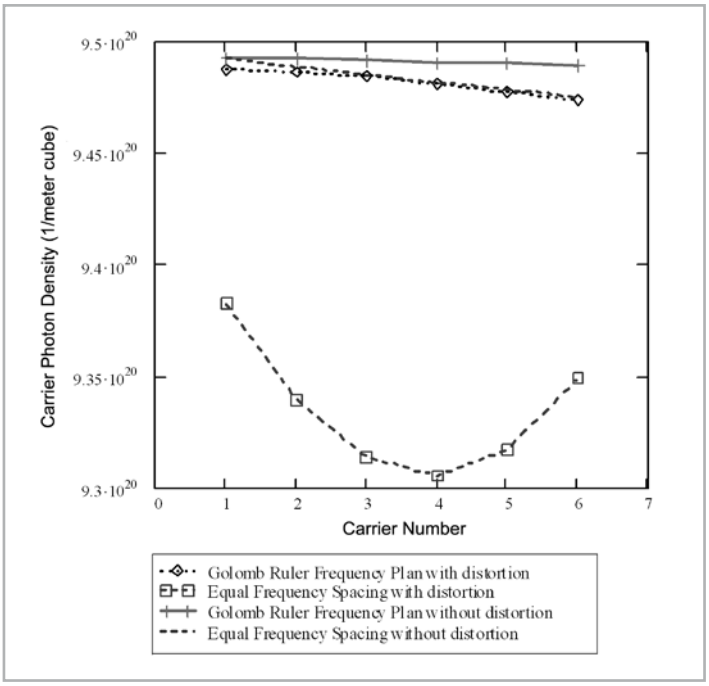

Figure 14 : The distorted and undistorted carriers at the bias current of 0.44A

Another way of evaluating the IMDs' effect on the carriers is to use the carrier-to-IMD (CIMD) ratio, given in Figures 15 and 16. The CIMD ratio trends for the both frequency plans are very different. The CIMD ratio for the GRFP decreases with the carrier numbers. The CIMD ratio for the EQSP minimises at the fourth carrier for both bias current. On the whole, the CIMD ratios were improved or increased when 0.44A was employed. The CIMD ratios of both frequency plans are also compared to the composite triple beat (CTB) and composite fifth order (CFO) in Figures 14 and 15. The composite triple beat (CTB) is the carrier to total IMD_3s in a channel [18]. The composite fifth order (CFO) refers to the carrier to total IMD_5s in a channel for this paper.

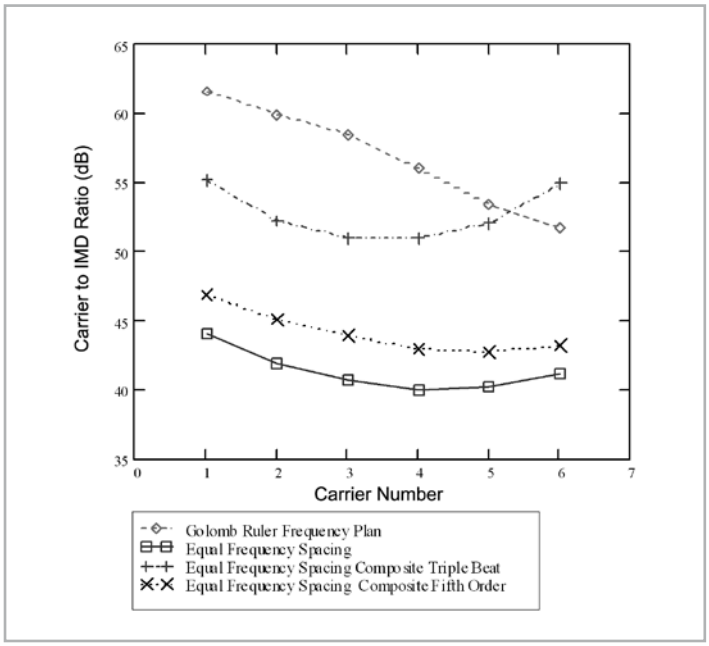

Figure 15 : The carrier to IMD ratios, CTB and CFO for both frequency plans at 25mA

The GRFP's CIMD ratios are higher than the EQSP for both bias current cases as it led to only IMD_5s at the carrier positions. The GRFP's CIMD ratios from 51.66 to 61.59dB and 55.63 to 65.56dB when 25*mA* and 0.44A bias current were employed. The CIMD ratio differences between both frequency plans ranged from 10.5 to 18.02dB at 25*mA*. The EQSP's CIMD ratios were 18.04 and 27.8dB lower than those of the GRFP. The CIMD ratios for the GRFP exceed the EQSP's CTB for all carrier number at 25mA bias current, except at the fourth. This is because the composite IMD_5 level at the fourth carrier of the GRFP was higher the composite IMD_3 level of the EQSP.

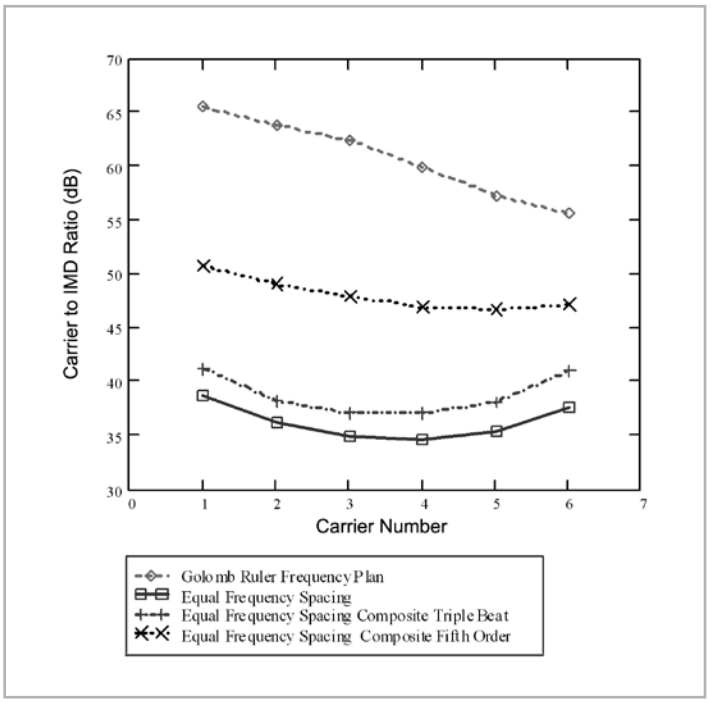

Figure 16 : The carrier to IMD ratios, CTB and CFO for both frequency plans at 0.44A

The EQSP's CIMD ratio curve resembled and appeared nearer to its CFO than its CTB as its composite IMD_5 levels were higher than its composite IMD_3 levels. In addition, this also caused the EQSP CFOs to be lower than its CTBs. The EQSP's CFO curve was below the GRFP's CIMD trend at 0.44A. The EQSP's CIMD ratio curve resembled and appeared nearer to its CTB than its CFO as its composite IMD_3 levels were higher than its composite IMD_5 levels.

High CIMD ratio is desired as they indicate that the carriers are less suppressed by the distortions. The CIMD is important especially when the signal strength is used in mobile communications to decide whether calls are to be handoff or avoidance of call drop. One of the criterias for handoff to take place in the mobile communications is the carrier to interference ratio of 18dB [5]. The sources of interference can come from co-channel interference. However the situation can be worsened when the co-channel interference is coupled with the distortions from the optical link. Therefore the distortions that cannot be filtered from the E/O should be minimised and this can be done using the GRFP and higher bias current. As such, the GRFP would be a better candidate than the equal frequency spacing to be incorporated into the SEFA.

5.0 CONCLUSION

The GRFP led to no IMD_3 and less IMD_5 levels to appear at carrier positions as compared to the equally spaced carriers. This in turn resulted in high CIMD ratios. As such, the GRFP can be used together with the SEFA and SLC schemes before the E/O conversion stage of the radio-over-fibre system. However, one problem might arise from deploying the GRFP. As the number of channels to be used increases, the bandwidth occupied by the GRFP can exceed that of the equal frequency spacing and lead to interference with signal designated in other bands for the radio-over-fibre system providing multi-band services. An alternative to this is to employ the optimum Golomb Ruler (OGR) that can lead to slightly reduced bandwidth consumption. Another option is to utilise a sub-optimal Golomb Ruler with a higher bias current, if the OGR is not available. This might lower the carrier position IMD levels and consume less bandwidth. ■

REFERENCES

[1] International Telecommunications Union Recommendation ITU-RF.1332-1* Radio-Frequency Signal Transport Through Optical Fibres., 1997-1999.

[2] H. Al-Raweshidy and S. Komaki, Radio over fiber technologies for mobile communications networks (Boston: Artech House, 2002).

[3] M. Fujise and H. Harada. "An Experimental Study on Multi-service Radio on Fiber Transmission System for ITS Road-Vehicle Communications", IEEE MWP'99 Digest, pp. 261-264, 1999.

[4] T. S. Chu and M. J. Gans, "Fiber Optic Microcellular Radio", IEEE Transaction on Vehicular Technology, vol.40, No. 3, pp. 599-606, 1991.

[5] W. C. Y. Lee, Mobile cellular telecommunications – analog and digital systems. 2nd ed., New York: McGraw Hill, 1995.

[6] L.K. Chen, K.Y. Lau and Y. Trisno, Frequency planning for nonlinear distortion reduction in wideband transmission, Electronics Letters, Vol.27, No.14, pp.1293 – 1295, 1991.

[7] C.-K. Chan, L.-K. Chen, Efficient frequency assignment scheme for intermodulation distortion reduction in fibre-optic microcellular systems, Electronics Letters, Vol. 30, No. 22, pp.1831 – 1832, 1994.

[8] Y. Aburakawa and H.Ohtsuka, Signal extraction with frequency arrangement (SEFA) and superimposed subcarrier modulation (SSM) schemes in fiber-oriented wireless access systems, Journal of Lightwave Technology, Vol.15, No.12, pp.2223 – 2231, 1997.

[9] M. Ogasawara, O. Kagami and H. Ichikawa, Analysis and measurement of effects of SCM techniques in WLL systems, Proc. IEEE Globecom 1998 3, Sydney, pp.1479-1484, 1998.

[10] J. B. Shearer, IBM Corporation, 2001. 19 Dec. 2003 <http://www.research.ibm.com/people/s/shearer/grap.html>

[11] Project OGR, DISTRIBUTED COMPUTING TECHNOLOGIES INC (distributed.net), 2003. 11 May 2004 <http://www1.distributed.net/ogr/ >

[12] Choi, In-Hyuk, Sang-Hoon Lee, Hyuk-Choon Kwon, Young-Wan Choi, and Sang-Kook Han. (2006) "Compensation of Intermadulation Distortion of Laser Diode By Using Optoelectronically Predistorted Signals", Microwave and Optical Technology Letters, Vol. 48, No. 6, Wiley Periodicals, Inc. 2007, pp.1144 – 1148, 2007.

[13] M.K. Hong, and S.K. Han "All Optical Linearization Technique of DFB-LD Based on Optical Injection Locking for RoF System", Microwave and Optical Technology Letters, Vol. 49, No. 10. Wiley Periodicals, Inc. 2007, pp. 2403 – 2406, 2007.

[14] N. Tayebi, and M. Kavehrad. (Sept.) Laser Nonlinearity Compensation for Radio Subcarrier Multiplexed Fiber Optic Transmission Systems, IEICE Trans. Commun., Vol. E76-B, No. 9, 1103-1114, 1993.

[15] T. K. Biswas, and W. F. McGee. Volterra Series Analysis of Semiconductor Laser Diode, IEEE Photonics Technology Letters, Vol. 3, No.8, pp. 706 –708,1991.

[16] S. A. Maas, Nonlinear microwave circuits, New York: IEEE Press, 1997.

[17] R. Ohmoto, H. Ohtsuka and H. Ichikawa, Fiber-optic microcell radio systems with a spectrum delivery scheme, IEEE Journal On Selected Areas in Communications, Vol.11, No.7, pp. 1108-1117, 1993.

[18] G. Keiser, Optical fiber communications. 3rd ed., Boston: McGraw Hill, 2000.

[19] H. M. Salgado and J. J. O'Reilly, Experimental validation of Volterra series nonlinear modelling for microwave subcarrier optical systems, IEE Proc. Optoelectron., Vol. 14, No. 4, pp. 209-213,1996.

[20] B. Pucel, "Comparison between Static and Dynamic Clipping Distortion in Semiconductor Lasers", IEEE Photonics Technology Letters, Vol.9, No.11, pp.1532-1534, November 1997.

PROFILE

LISA YONG

Lisa Yong received her BEng. (Hon.) in Electronics and Telecommunications Engineering and Master of Engineering in Electronics and Telecommunication Engineering from Universiti Malaysia Sarawak. She currently a lecturer at the School of Engineering and Science, Swinburne University of Technology (Sarawak Campus), Kuching. Her research interests include radio-over-fibre systems, non-linear distortion modelling and linearization and renewable energy.